NUMERICAL SOLUTIONS OF THE COMPRESSIBLE 3-D BOUNDARY-LAYER EQUATIONS FOR AEROSPACE CONFIGURATIONS WITH EMPHASIS ON LFC

Julius E. Harris
NASA Langley Research Center
Hampton, Virginia

Venkit Iyer
Vigyan Research Associates, Incorporated
Hampton, Virginia

Samir Radwan
High Technology Corporation
Hampton, Virginia

[redacted]

THREE-DIMENSIONAL BOUNDARY-LAYER PROGRAM
LAMINAR FLOW CONTROL RESEARCH
NASA LANGLEY RESEARCH CENTER

The application of stability theory in Laminar Flow Control (LFC) research requires that density and velocity profiles be specified throughout the viscous flow field of interest. These profile values must be as numerically accurate as possible and free of any numerically induced oscillations. To date, a high percentage of the boundary-layer solutions for use in three-dimensional (3-D) stability analysis programs have been obtained using quasi-3-D procedures due to the general unavailability of 3-D boundary-layer programs.

Several mature 3-D boundary-layer programs based on finite-difference techniques (note: integral approaches are not considered in the present paper) currently exist, for example, references 1 through 4. Unfortunately, these programs are not available for general use by the LFC research community due to company proprietary controls. In addition to proprietary controls, most of the programs are not structured or adequately documented for ease of use; that is, their use would generally require direct interaction with and/or assistance from the group or individual that developed the program.

Guidelines for the present research project are presented in figure 1 and are as follows: (1) develop an efficient and accurate procedure for solving the 3-D boundary-layer equations for aerospace configurations; (2) develop an interface program to couple selected 3-D inviscid programs that span the subsonic to hypersonic Mach number range; and (3) document and release software to the LFC research community.

- Reasons for development
  - No general program exists that is readily available to all groups involved in laminar flow control research
  - No general program exists that is coupled directly with the most often used inviscid programs over the subsonic to hypersonic Mach number range
  - Most existing programs are at best second-order accurate and often degenerate to first-order accuracy
- Guidelines for development
  - User friendly
  - High-order accuracy; $O(\Delta Z^4)$, $O(\Delta X, \Delta Y)^2$
  - Flexible interface
  - Document and release to LFC Research community

(Finite difference numerics)

FIGURE 1

ORDER OF PRESENTATION

As a result of time constraints for the present symposium, it was necessary to condense the material that would have been included in three presentations into a simple co-authored paper. Consequently, no attempt will be made to either (1) give a review of current boundary-layer literature or (2) compare numerical results from the present solution procedure with previously published numerical and/or experimental results. The material to be presented is outlined in figure 2 and is divided into two basic categories. The interaction between these categories will not be discussed due to time limitations.

Within the inviscid area the focus of the presentation will be on the processing of the inviscid flow field data required as input to the boundary-layer program. The surface Euler equations will be defined together with the numerical procedure for solving the nonlinear system. Several test cases will be presented where results obtained from standard interpolation procedures will be compared with results from the surface Euler equations.

Within the viscous area the focus of the presentation will be on the numerical procedure and the establishment of its accuracy and numerical efficiency. The boundary-layer equations will not be presented in equation form; however, their mathematical character and the required boundary and initial conditions will be discussed. The reader interested in the full equations can find them in several publications (see refs. 1 through 6, for example).

- Inviscid
  - Interface program
  - Inviscid data treatment
  - Surface Euler equations
    - Boundary conditions
    - Numerical procedure
  - Test cases
- Viscous
  - Governing equations
    - Boundary conditions
    - Initial conditions
    - Transformation
  - Solution technique
    - Numerical scheme
    - Matrix structure
  - Test cases

FIGURE 2

INTERFACE PROGRAM

The interface program provides the required linkage between the most appropriate inviscid code for the configuration and flight Mach number regime and the three-dimensional boundary-layer program. The functions of the interface program are presented in figure 3. The interface program must be capable of (1) generating a sufficiently refined boundary-layer grid; (2) calculating the metric coefficients and related geometric parameters for this grid; (3) interpolating the pressure field from the relatively coarse grid used for the inviscid flow field solution to the relatively fine boundary-layer grid with automatic smoothing capability as required; (4) solving the surface Euler equations on the wall boundary to obtain the inviscid velocity components and their gradients in the ξ, η coordinate system; and (5) generating all required input files for the boundary-layer program. In addition to these primary functions, the interface program prepares diagnostic plot files and will act as the interactive link for viscous-inviscid interaction calculations.

Success (measure of acceptance and use of software by LFC research groups) of the boundary-layer program will depend, to a large extent, on the structure of the interface software.

- General function
  - Provide the required linkage between selected inviscid programs that span the subsonic to hypersonic Mach number range and the boundary-layer program under development
- Specific functions
  - Generation of boundary-layer grid and related metric coefficients
  - Interpolation of inviscid pressure distribution from the relatively coarse inviscid grid to the sufficiently fine boundary-layer grid
  - Solution of the surface Euler equations to obtain the inviscid velocity distribution over the boundary-layer grid
  - Generation of input and output files for the boundary-layer program
  - Interface for viscous-inviscid interaction

FIGURE 3

TREATMENT OF INVISCID DATA

The sensitivity of stability theory to oscillations in the viscous flow field requires that the inviscid data and body geometry (metric coefficients, etc.) be carefully treated in order to avoid the introduction of nonphysical oscillations. Alternate approaches to inviscid flow-field data treatment are presented in figure 4. A conventional approach has been to use spline interpolation to transfer data from the relatively coarse inviscid grid to the sufficiently fine boundary-layer grid. These interpolated results are then numerically smoothed. The interpolation approach is the most straightforward; however, large errors can occur in the interpolation and arbitrary smoothing of vector quantities. This approach yields results that are not consistent; that is, they do not satisfy the governing inviscid equations within an acceptable error bound.

The present approach is to interpolate the pressure field from the coarse inviscid grid to the fine boundary-layer grid. This pressure distribution $P_w(\xi,\eta)$, together with known initial and boundary values, is used in the numerical solution of the surface Euler equations. The advantage of the approach is that exact values of u and v can be enforced on certain boundaries, the velocity components (u,v) and their gradients in the ξ,η plane are smooth, and the numerical results are consistent.

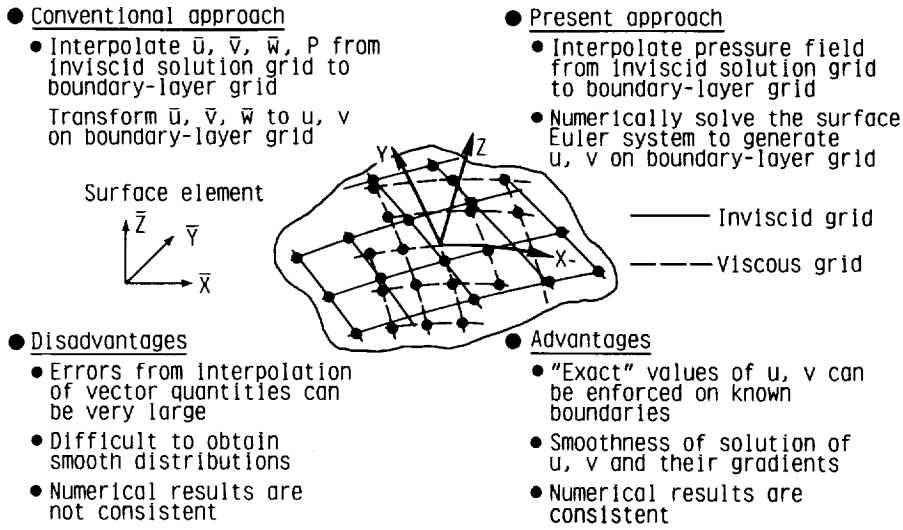

FIGURE 4

SURFACE EULER EQUATIONS

The surface Euler equations are obtained from the three-dimensional boundary-layer equations in the limit as $\zeta \to \infty$. The system obtained from the ξ and η momentum equations are presented in figure 5. The system consists of two nonlinear hyperbolic equations for the ξ and η momentum equations and an algebraic relationship for the energy equation (perfect gas). The $b_{k\ell}$ values are known functions of the grid system. The pressure is known from the interpolation procedure. The unknowns are ρ, u, and v, where ρ, u, and v are the density, ξ-velocity component, and η-velocity components, respectively. The equations are a first order, nonlinear hyperbolic system where the local streamlines are characteristic. The system can be solved with an explicit march in ξ while remaining fully implicit in η provided the initial conditions and boundary conditions can be specified as indicated in figure 5.

A method for calculating the inviscid velocity vectors from a specified pressure field was first reported by Cebeci and Meier (ref. 6) for incompressible flow around an ellipsoid at angle of attack. Vollmers (ref. 7) and Gleyzes and Cousteix (ref. 8) improved the approach by integrating the Euler equations. Anderson (ref. 3) described a method using experimental pressure distributions on rotating turbine blades using the Euler equations. The current procedure extends these concepts to complex geometry associated with wings and fuselages using a second-order numerical scheme.

- Equation system obtained from boundary-layer equations in limit as $\zeta \to \infty$
- Equations

  ξ-momentum

$$\rho[b_{11}u\frac{\partial u}{\partial \xi} + b_{12}v\frac{\partial u}{\partial \eta} + (b_{12}u^2 + b_{14}uv + b_{15}v^2)] = (b_{16}\frac{\partial P}{\partial \xi} + b_{17}\frac{\partial P}{\partial \eta})$$

  η-momentum

$$\rho[b_{21}u\frac{\partial v}{\partial \xi} + b_{22}v\frac{\partial v}{\partial \eta} + (b_{23}u^2 + b_{24}uv + b_{25}v^2)] = (b_{26}\frac{\partial P}{\partial \xi} + b_{27}\frac{\partial P}{\partial \eta})$$

- Character of system
  - First order, nonlinear hyperbolic system
  - Local streamlines are characteristics
    - Explicit march in ξ; implicit in η

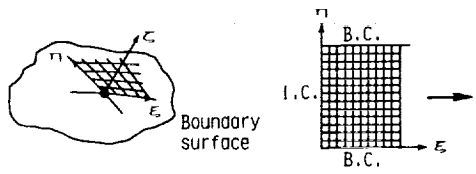

FIGURE 5

BOUNDARY CONDITIONS FOR FUSELAGE "TYPE" GEOMETRY

As previously noted in figure 5, initial and boundary conditions must be specified for physical flows corresponding to aerospace configurations. These conditions are presented in figure 6(a) for a fuselage type body. The fuselage type body with a plane of symmetry relative to the flow field has well defined initial and boundary conditions. The initial conditions at the stagnation point in the physical plane are $u = v = 0$. These conditions from the required initial values along the $\xi = \xi_o$ line in transformed space. Along both the leeward and windward lines of the symmetry plane in physical space one can specify the conditions $v = 0$ and $\partial u/\partial \eta = 0$. These form the boundary conditions in the transformed plane for the lines $\eta = \eta_o$ and $\eta = \eta_{max}$.

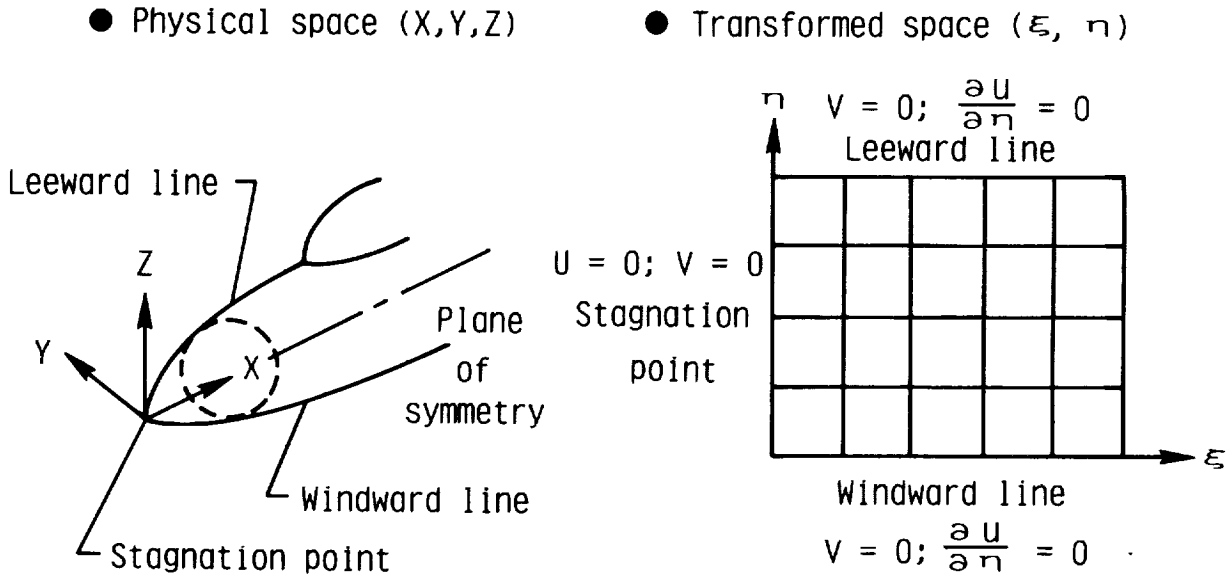

FIGURE 6(A)

BOUNDARY CONDITIONS FOR WING GEOMETRY

Boundary and initial conditions for wing type geometry are somewhat more complex than those for fuselages. A schematic of a typical wing element is presented in figure 6(b) where α and Λ denote the angle of attack and leading-edge sweep, respectively. At angle of attack, the leading-edge attachment line will be displaced from the geometrical leading edge as shown in the sketch. The location of the attachment line is not known a priori and must be obtained by an iterative solution procedure that positions the line such that $u = 0$ to within a specified error bound. This becomes the $\xi = \xi_o$ line in the transformed plane. The remaining initial condition along the $\xi = \xi_o$ line is obtained from the inviscid flow field results (see ref. 9). The boundary conditions along either the root chord or symmetry plane chord and a chord near, but not located at the wing tip, must be specified. The extrapolation conditions shown in the ξ, η plane in figure 6(b) for the wing tip and root chord regions have been used for the results contained in the present material. A more detailed discussion of the initial conditions for the leading-edge attachment line and boundary condition studies for the wing tip and root regions is presented in reference 9.

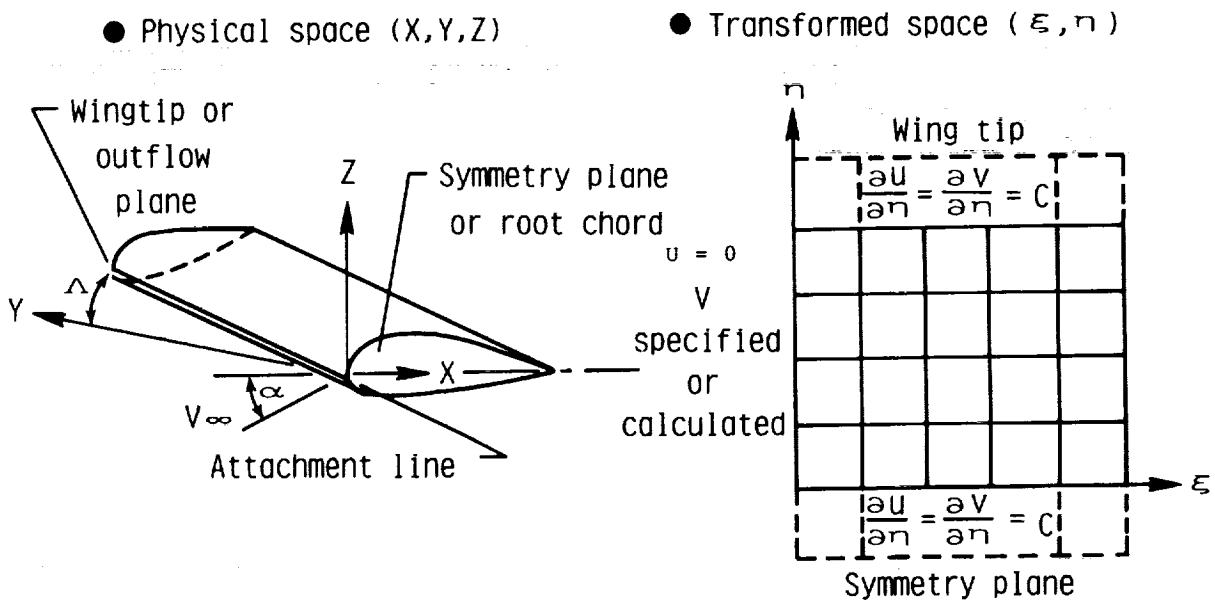

FIGURE 6(B)

NUMERICAL PROCEDURE

As previously mentioned, the surface Euler equations are hyperbolic. In order to satisfy the stability requirement, the difference stencil must be rotated in relation to the cross flow velocity as shown in figure 7(a).

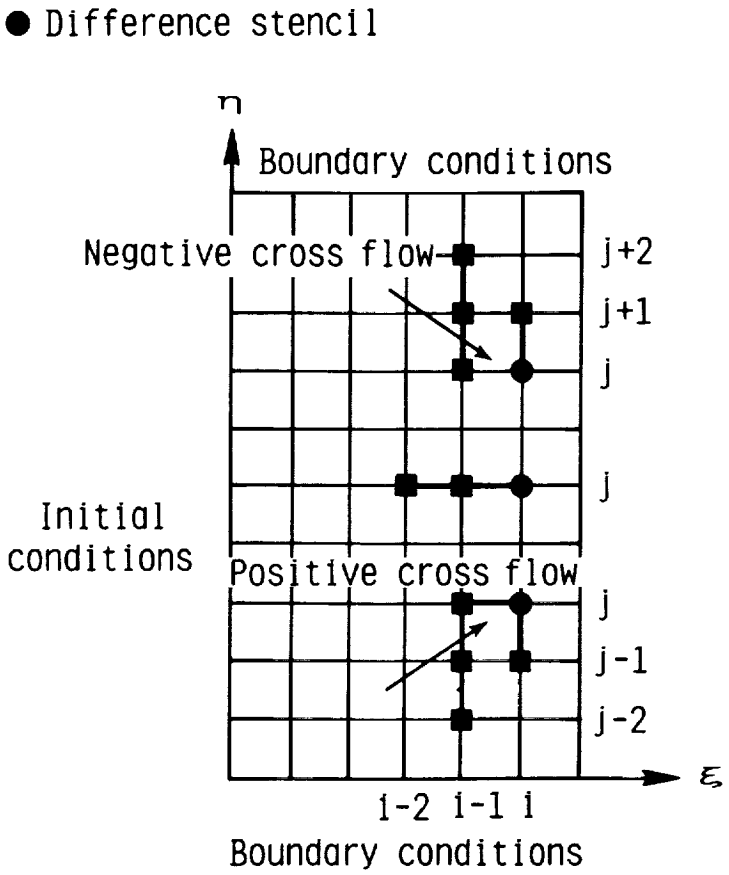

FIGURE 7(A)

DIFFERENCE APPROXIMATIONS

The point upwind differences are used to approximate derivatives with respect to ξ (see fig. 7(b)). For derivatives with respect to η a 5-point stencil is used and rotated to satisfy stability where e = 1 for v < 0; e = -1 for v > 0.

Nonlinear terms are treated in an iterative sense by lagging the nonlinear quantity by one iterative step. The final set of discretized equations are "locally block diagonal."

$$\frac{\partial f}{\partial \xi_{i,j}} = \frac{1}{(\xi_{i,j} - \xi_{i-1,j})} \left\{ f_{i,j}(1+g) - \frac{f_{i-1,j}}{(1-g)} + f_{i-2,j} \frac{g^2}{(1-g)} \right\}$$

$$g = \frac{(\xi_{i,j} - \xi_{i-1,j})}{(\xi_{i,j} - \xi_{i-2,j})}$$

$$\frac{\partial f}{\partial \eta_{i,j}} = \frac{1}{(\eta_{i,j} - \eta_{i,j+\epsilon})} \left\{ f_{i,j} - f_{i,j+\epsilon} + \frac{f_{i-1,j}}{1+\lambda} - \frac{f_{i-1,j+\epsilon}}{\lambda} + \frac{f_{i-1,j+2\epsilon}}{\lambda(1+\lambda)} \right\}$$

$$\lambda = \frac{\eta_{i-1,j+\epsilon} - \eta_{i-1,j+2\epsilon}}{\eta_{i,j} - \eta_{i,j+\epsilon}}$$

$$\epsilon = +1 \quad v < 0$$

$$\epsilon = -1 \quad v > 0$$

FIGURE 7(B)

PRESSURE COEFFICIENT CONTOURS

A test case of interest to the Langley Research Center's LFC program involves experimental and analytical studies of the stability characteristics of a fuselage forebody shown in figure 8. Figure 8(a) presents contours of the pressure coefficient distribution interpolated from a relatively coarse inviscid solution onto a fine boundary-layer grid. The initial inviscid distribution was obtained using the method of reference 10.

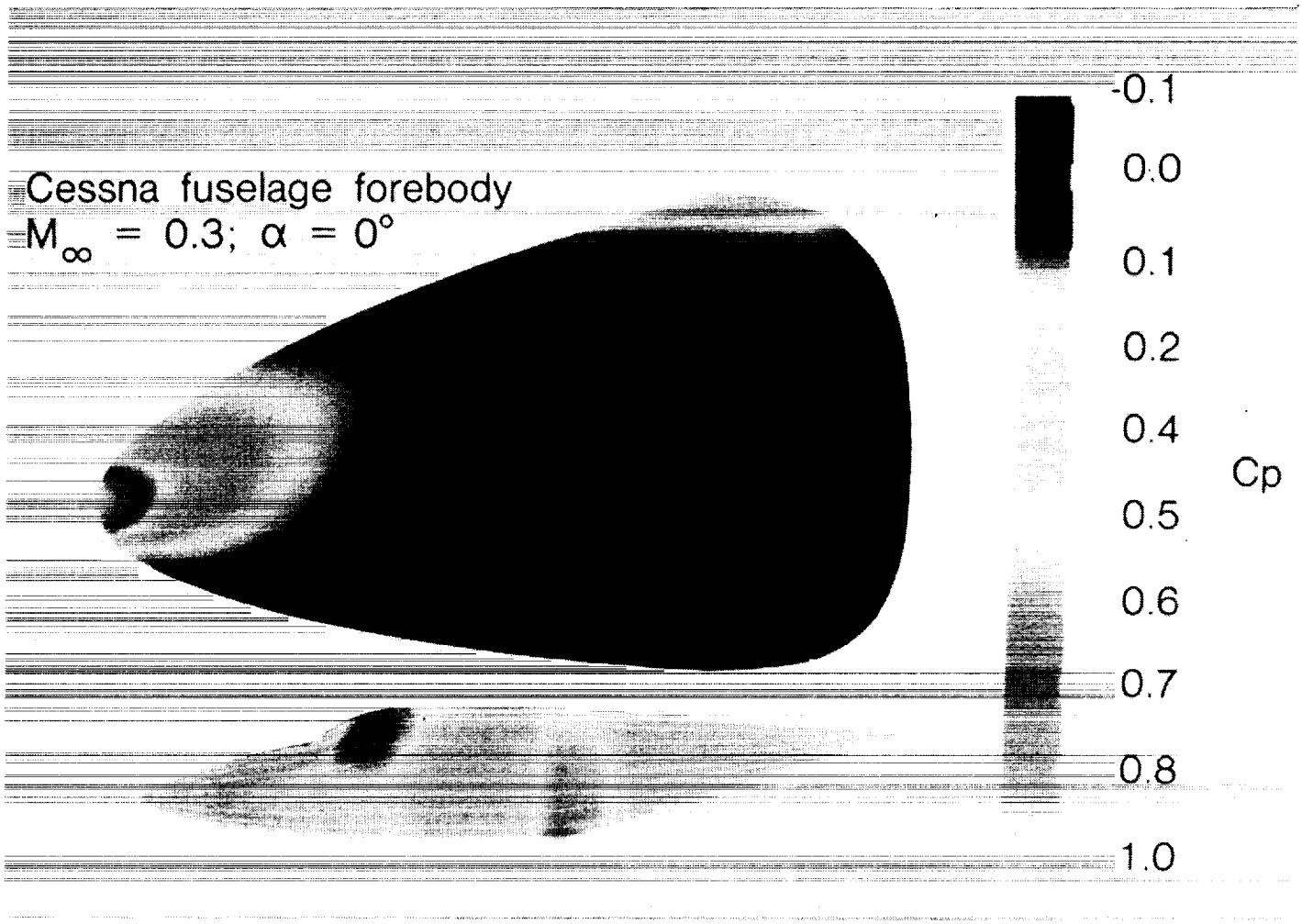

FIGURE 8(A)

INVISCID FLOW-FIELD CONTOURS

The pressure contours in figure 8(a) indicate a smooth and "well behaved" flow field; however, close examination of the cross flow velocity contours in figure 8(b) indicates a physical problem not easily solved by traditional boundary-layer procedures. The solid line on figure 8(b) indicates the locus of a $v = 0$ contour line. In the region above this line $v > 0$ (positive cross flow) while below the line $v <$ (negative cross flow). Consequently, both the leeward and windward lines of the plane of symmetry are inflow lines. This presents a severe problem for traditional boundary-layer approaches where one normally obtains a numerical solution of the reduced set of boundary-layer equations along the windward line (generally an outflow line). Using this solution as one of the two required initial data planes, the solution can be marched in the direction of increasing η (direction of positive cross flow velocity) to obtain the solution for $\xi = \xi_i$, $\eta_o < \eta \leq \eta_{max}$, and all ζ. The surface Euler equations could be numerically integrated for $\xi = \xi_i$, $\eta_o < \eta < \eta_{max}$ because the entire η-line was treated implicitly.

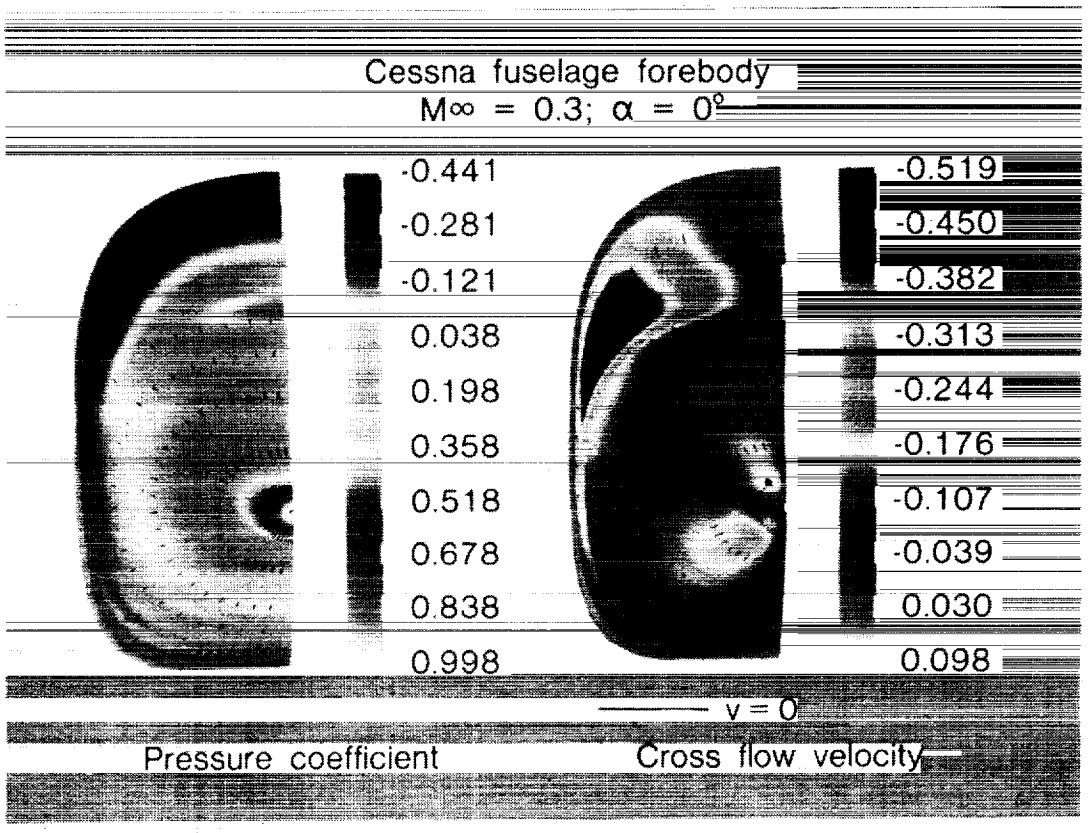

FIGURE 8(B)

SURFACE EULER VERSUS STANDARD INTERPOLATION

Comparisons of interpolated u and v values with those obtained from solving the surface Euler equations are presented in figure 9. The interpolated values were carefully smoothed to get the results presented in figure 9(a) as opposed to no smoothing for the velocity field obtained from the surface Euler equations. In addition, the interpolated values are not consistent.

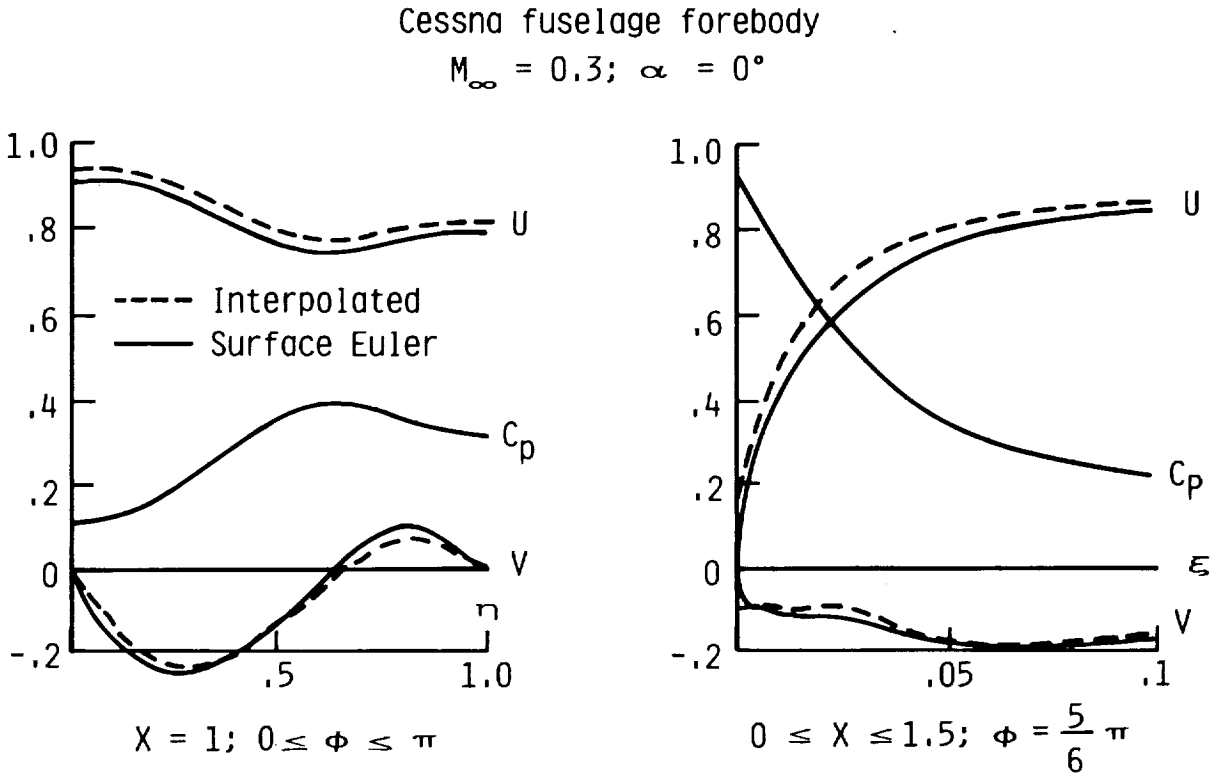

FIGURE 9(A)

CROSS FLOW VELOCITY CONTOURS

The carpet plots of cross flow velocity presented in figure 9(b) are indicative of oscillations resulting from interpolation of the velocity components. Stability theory is critically sensitive to oscillations of cross flow velocity; consequently, the surface Euler approach should be used to obtain smooth and consistent input data for the boundary-layer solution.

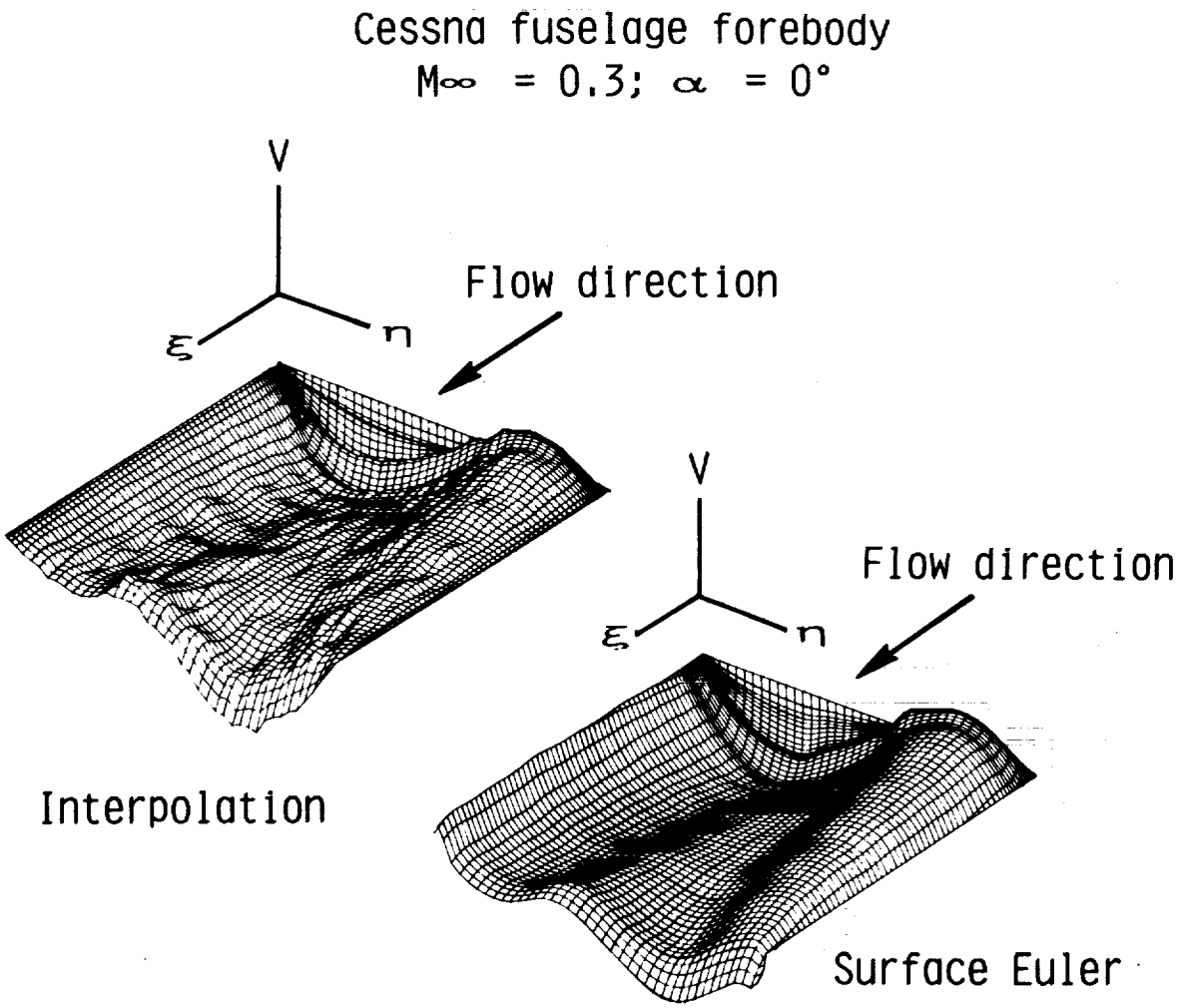

FIGURE 9(B)

COMPARISON OF SURFACE EULER WITH INTERPOLATION

Numerical results are presented in figure 10 for a wing having an NACA-0012 airfoil section. The inviscid flow field was obtained using the method of reference 10. Comparisons of the interpolated and smoothed streamwise velocity are compared with surface Euler results in figure 10(a). The agreement in magnitude appears to be satisfactory with the exception of a region just downstream of the leading-edge attachment line. The agreement appears to be independent of span location.

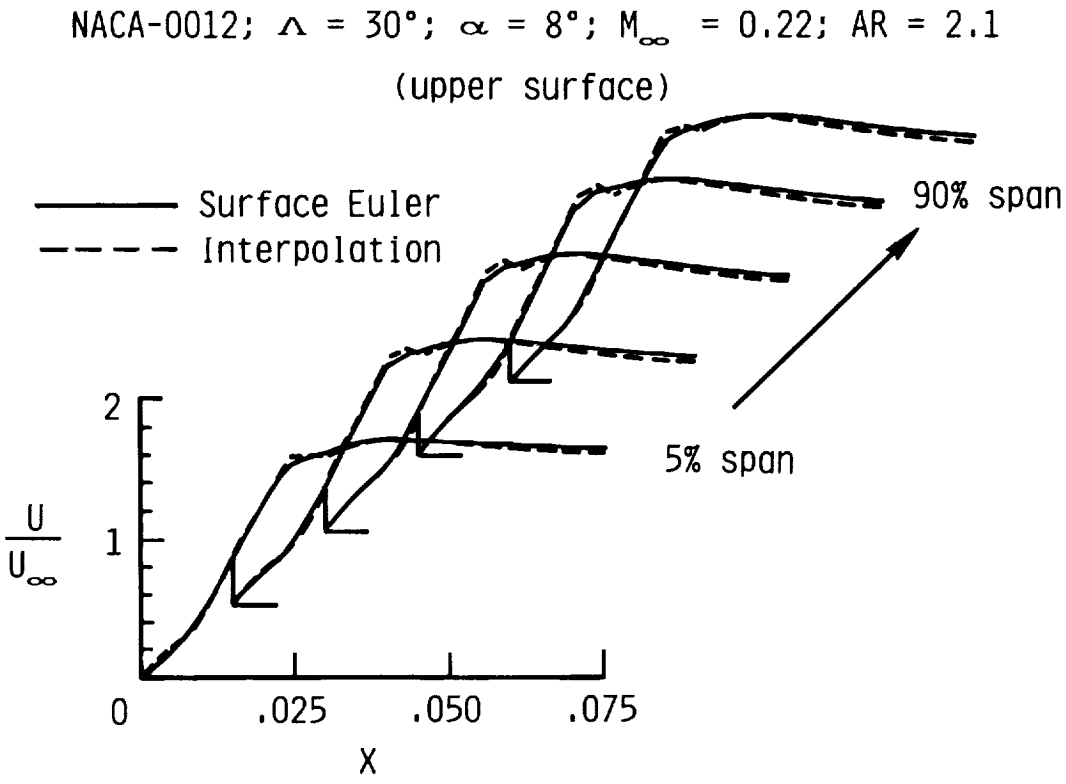

FIGURE 10(A)

COMPARISON OF SURFACE EULER WITH INTERPOLATION

The stability equations will be integrated forward in space beginning at the leading-edge attachment line. A closer examination of the results presented in figure 10(a) is presented as a derivative with respect to x in figure 10(b). The oscillation in $\partial\tilde{U}/\partial\xi$ presented in figure 10(b) for the interpolated values is not acceptable. It can be seen that the surface Euler equations yield smooth values of $\partial\tilde{U}/\partial\xi$ without requiring smoothing. These values are consistent with the governing equations.

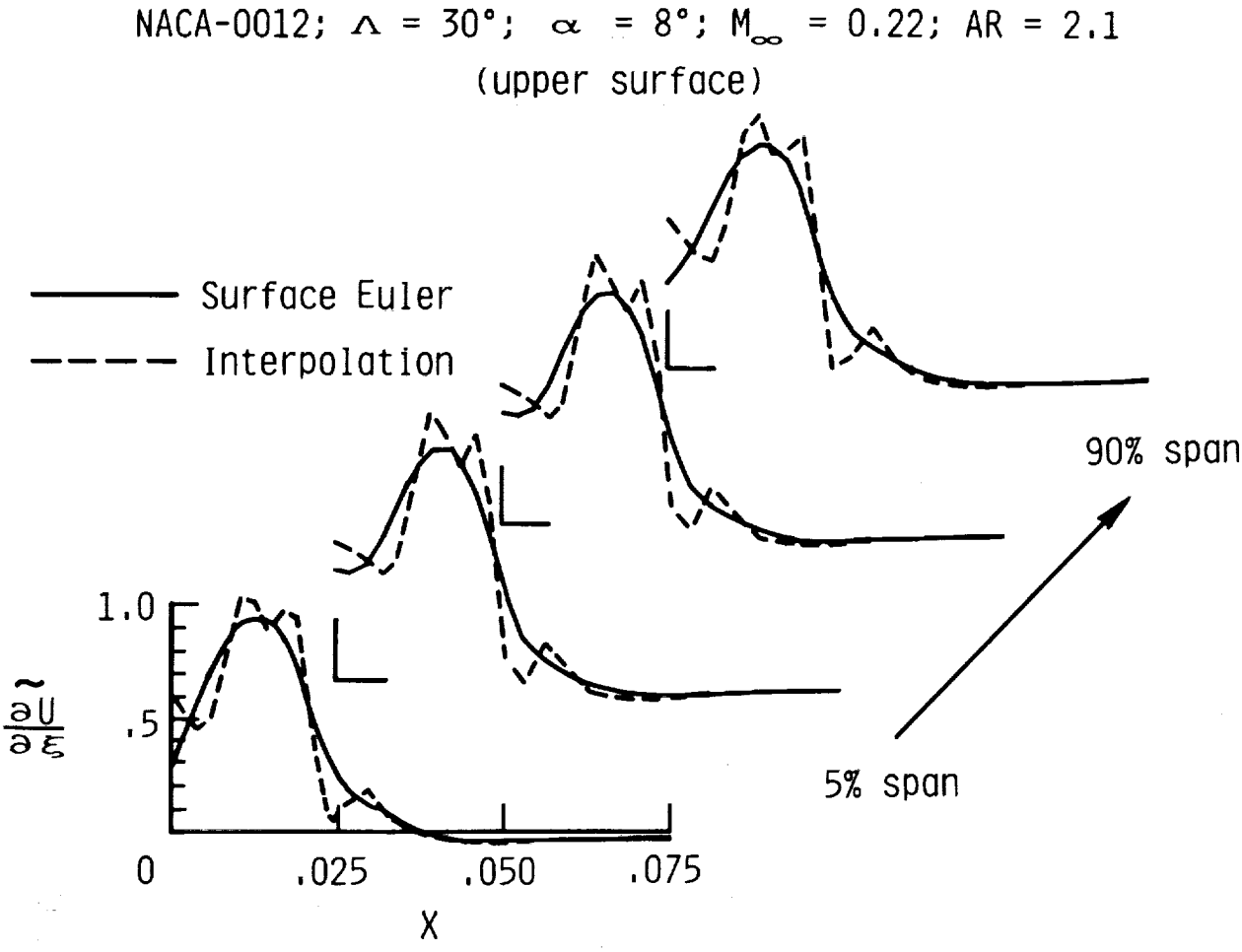

FIGURE 10(B)

THREE-DIMENSIONAL BOUNDARY-LAYER SYSTEM

Researchers involved in the numerical aspects of LFC are familiar with the three-dimensional boundary-layer equations; consequently, the equations are not presented. Readers interested in the equations are refered to references 1 through 5. Certain characteristics of the system are presented in figure 11 and warrant further discussion.

The system consists of four nonlinear partial-differential equations (PDEs) of mixed type. The system is hyperbolic in planes parallel to the boundary surface (ξ,η planes) and parabolic in the direction normal to these planes.

For perfect gas flow, the system is closed with algebraic equations for state and viscosity. The unknowns are u, v, w, T and ρ representing the velocity components in the ξ,η,ζ directions, static temperature and density, respectively. Pressure is constant normal to the wall boundary.

The present work focuses on laminar flow; however, the software has been structured to model the turbulent terms using eddy viscosity and eddy conductivity closure. Careful studies will be made in this area at some future date. This would allow a uniform approach for boundary-layer calculations to be developed for laminar, transitional, and turbulent flows.

- Equations
  - Continuity
  - Momentum (2; X, Y) } Nonlinear PDE
  - Energy
  - State; viscosity } Algebraic
- Turbulence
  - Eddy viscosity/eddy conductivity } Not LFC requirement

FIGURE 11(A)

THREE-DIMENSIONAL BOUNDARY-LAYER SYSTEM

Boundary conditions have been treated as generally as possible. Wall mass transfer can be specified together with either wall temperature or heat transfer distributions. Edge values are obtained from the interface software solutions of the surface Euler equations. Initial values can currently be generated for fuselage and wing geometries. The reader interested in the special equation sets for the initial value planes is referred to reference 5.

- Boundary conditions
  - Wall boundary
    - U; V (no slip)
    - $W_W = W_W (X,Y)$
    - $T_W = T_W (X,Y)$
      or $q_W = q_W (X,Y)$
  - Edge values
    - Surface Euler system
- Initial values
  - Fuselage "type" geometry
    - 3-D stagnation point
    - Symmetry plane
  - Wing "type" geometry
    - Leading edge attachment line
    - Symmetry plane
    - Root chord approximation

FIGURE 11(B)

NUMERICAL SCHEME

The difference stencil together with a sketch depicting the Raetz influence principle (ref. 5), and the difference approximations are presented in figure 12(a). Two separate stencils are used for convective derivatives in the ξ,η-plane. The particular stencil utilized at each ζ point depends upon the sign of the cross flow velocity. For negative cross flow the Krause et al. (ref. 11) zig-zag scheme is used to satisfy the zone of influence principle.

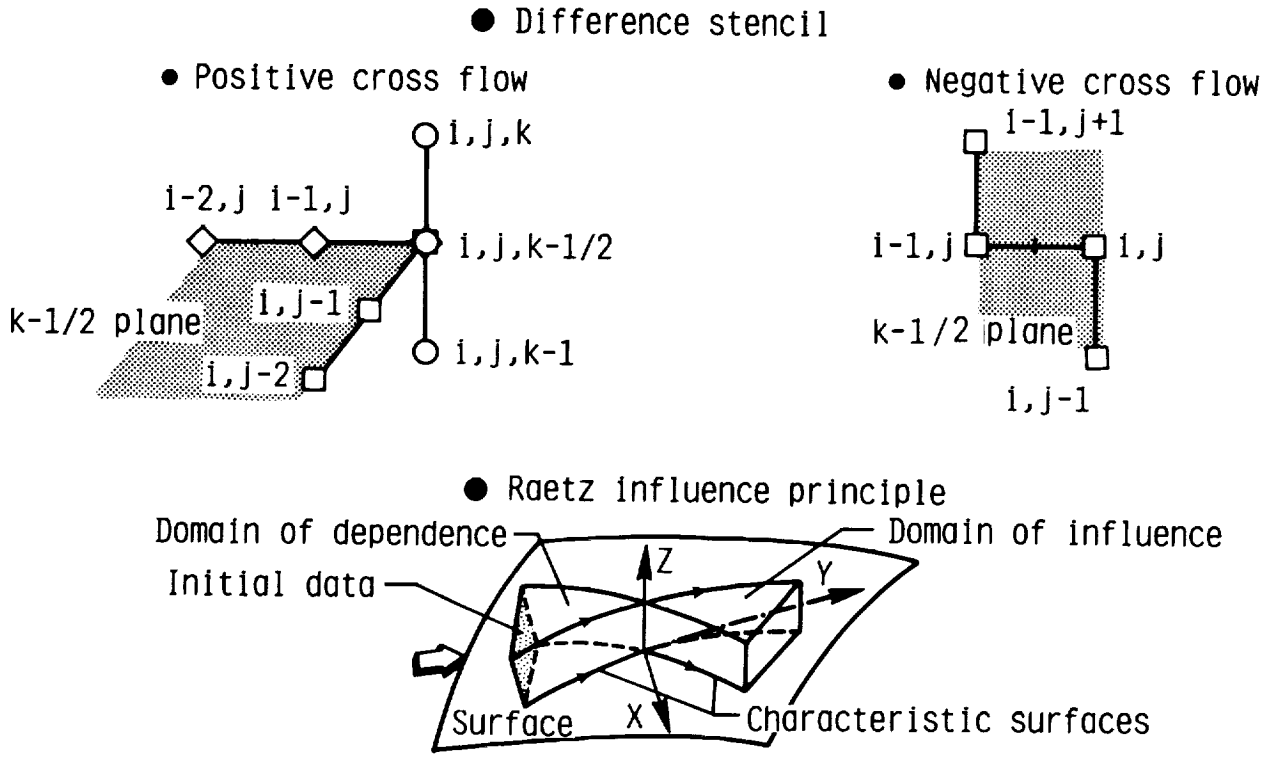

FIGURE 12(A)

DIFFERENCE APPROXIMATIONS

The difference approximations are presented in figure 12(b). The approximations are second-order accurate in planes parallel to the wall and fourth-order accurate in the direction normal to the wall boundary. In the planes parallel to the wall, a weighted three-point upwind scheme is used to approximate the convective partial-derivatives (see ref. 12).

In the direction normal to the wall boundary, a 2-point compact scheme with fourth-order accuracy is used (see refs. 13 and 14).

NUMERICAL SCHEME

Difference relations

- ξ - derivatives

$$\left(\frac{\partial \Phi}{\partial \xi}\right)^{k-\frac{1}{2}}_{i,j} = \left(a_1\Phi_i + a_2\Phi_{i-1} + a_3\Phi_{i-2}\right)^{k-\frac{1}{2}}_{j}$$

- η - derivatives

$$\left(\frac{\partial \Phi}{\partial \eta}\right)^{k-\frac{1}{2}}_{i,j} = \left(b_1\Phi_j + b_2\Phi_{j-1} + b_3\Phi_{j-2}\right) \qquad v > 0$$

$$\left(\frac{\partial \Phi}{\partial \eta}\right)^{k-\frac{1}{2}}_{i,j} = \left(c_1\Phi_{j-1} + c_2\Phi_j\right)^{k-\frac{1}{2}}_{i} + \left(c_3\Phi_j + c_4\Phi_{j+1}\right)^{k-\frac{1}{2}}_{i} \qquad v < 0$$

- ζ = derivatives

$$\left(\bar{Q}^k - \bar{Q}^{k-1}\right)_{i,j} - \Delta\zeta\left(g_1\bar{Q}'^{,k} + g_2\bar{Q}'^{,k-1}\right)_{i,j} - \Delta J^2\left(g_3\bar{Q}''^{k} + g_4\bar{Q}''^{k-1}\right)_{i,j} = O(\Delta\zeta)^4$$

where $\bar{Q}^k_{i,j}$ = Solution vector

FIGURE 12(B)

SOLUTION TECHNIQUE

Substitution of the difference relations into the transformed governing equations yields a set of seven nonlinear, coupled difference equations in seven unknowns (see fig. 13). Newton's method is used to linearize the system. The linearized system is solved using an efficient block-tridiagonal matrix inversion based on LU factorization.

The two momentum equations yield a 4x4 block tridiagonal system in F, F', G, G', where $F = u/ue$, $G = v/ve$, $F' = \partial F/\partial \zeta$ and $G' = \partial G/\partial \zeta$. The energy equation yields a 2x2 block for H and H'. The normal component of velocity, w is updated from the finite-difference form of the continuity equation. The system is solved in an iterative loop until convergence is obtained within a fixed error bound.

- Difference equations are coupled and nonlinear
- Newton's method used for linearization

$$\bar{Q}^P = \bar{Q}^{P-1} + \delta\bar{Q}^{P-1}$$

- The linearized system of equations in δQ forms a block tri-diagonal system of the form

$$\{A\}\,\overline{\delta Q}^{k-1} + \{B\}\,\overline{\delta Q}^{k} + \{C\}\,\overline{\delta Q}^{k+1} = \bar{R}^k$$

Where

$\{A\}$,...., $\{C\}$ are block matrices of system

$\vec{Q}$ is solution vector

4×4 block tri-diagonal for momentum eqs

2×2 block tri-diagonal for energy eq

W updated from difference form of continuity eq

FIGURE 13

ACCURACY OF METHOD

The results of a study of the accuracy of the numerical scheme together with the effect of the number of grid points normal to the wall boundary for a fixed ζ_{max} are presented in figure 14. The truncation error study for Blasius flow clearly indicates a slope of 4 to 1 as compared with 2 to 1 for the second-order scheme of reference 12.

The numerical advantage of the fourth-order method is shown for 3-D stagnation point flow where streamwise velocity profiles (u/u_e) are presented for a fixed ζ_{max} for 40, 16, and 8 points normal to the wall boundary (note that only a sample of the computed points is presented for clarity). Comparisons of the results for NPZ = 8 with NPZ = 40 indicate that the correct profile values can be predicted with as few as 8 points. This comparison represents a speed/storage advantage of 5 to 1.

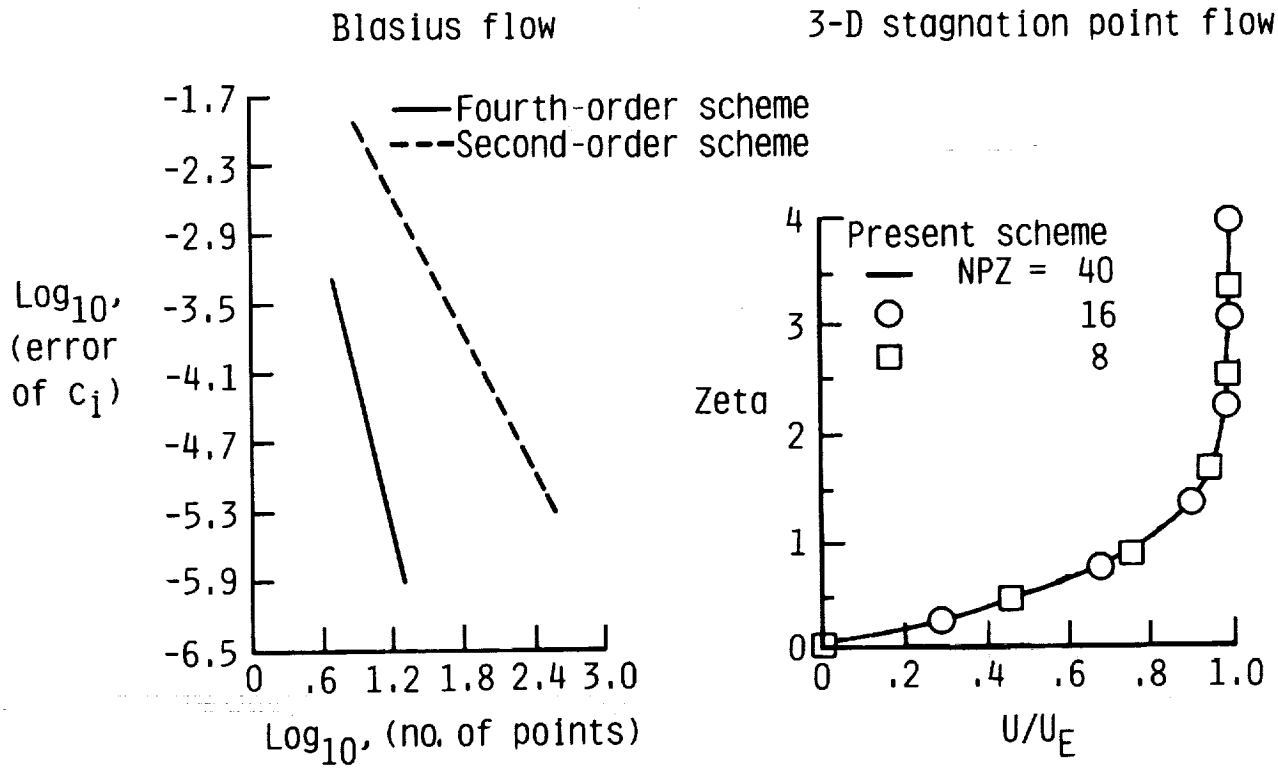

FIGURE 14

CYLINDER ON FLAT PLATE

Numerical results for incompressible flow past a cylinder mounted normal to a flat plate are presented in figure 15. Total and cross flow velocity profiles are presented for 50, 25, and 12 points normal to the wall as well as compared with the second-order theory of reference 12. The present fourth-order method produces excellent results for as few as 12 grid points normal to the wall boundary for this test problem.

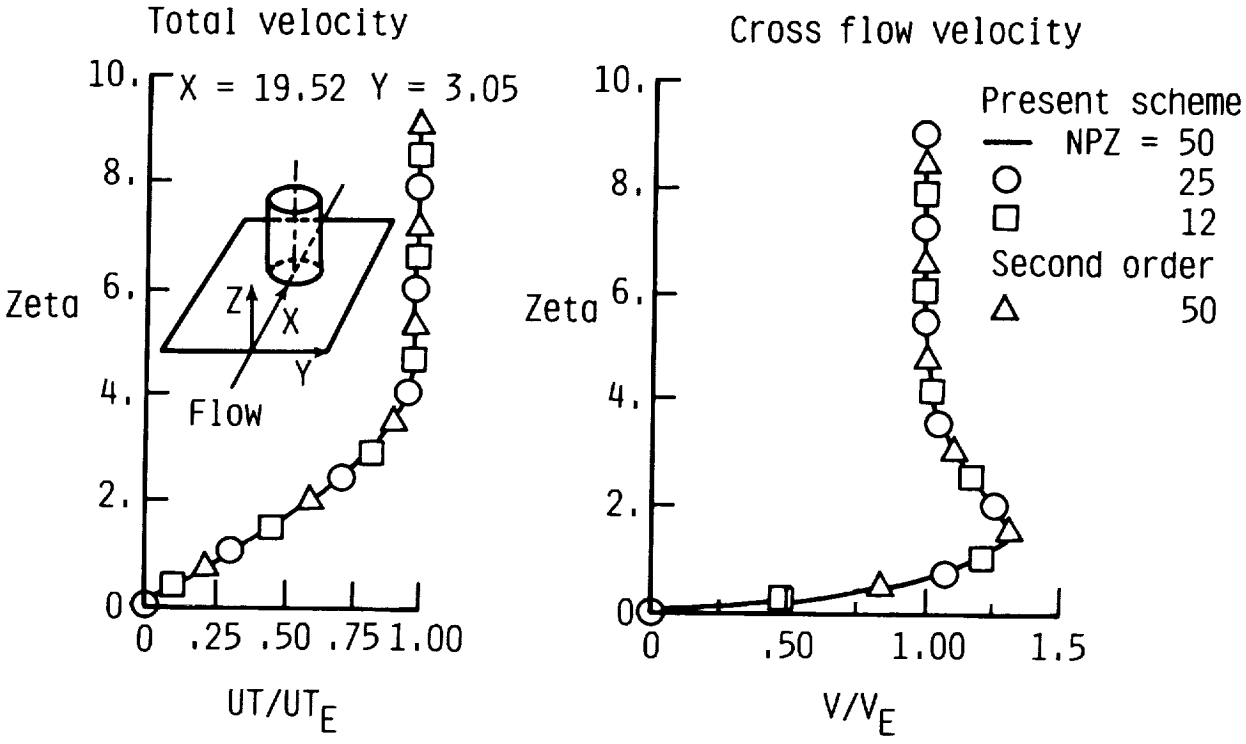

FIGURE 15

PROLATE SPHEROID AT ANGLE OF ATTACK

Numerical results for F'_w and G'_w for incompressible flow past a prolate spheroid at 8° angle of attack is presented in figure 16. The results are presented for three x locations where η varies from 0° on the most windward line of symmetry to 180° on the leeward line. Of particular importance is the reverse region of cross flow: $G'_w < 0$; $x = 1.52$; $60° < \eta < 180°$ (note that $G'_w = (\partial G/\partial \zeta)_w$; $G \equiv v/v_e$).

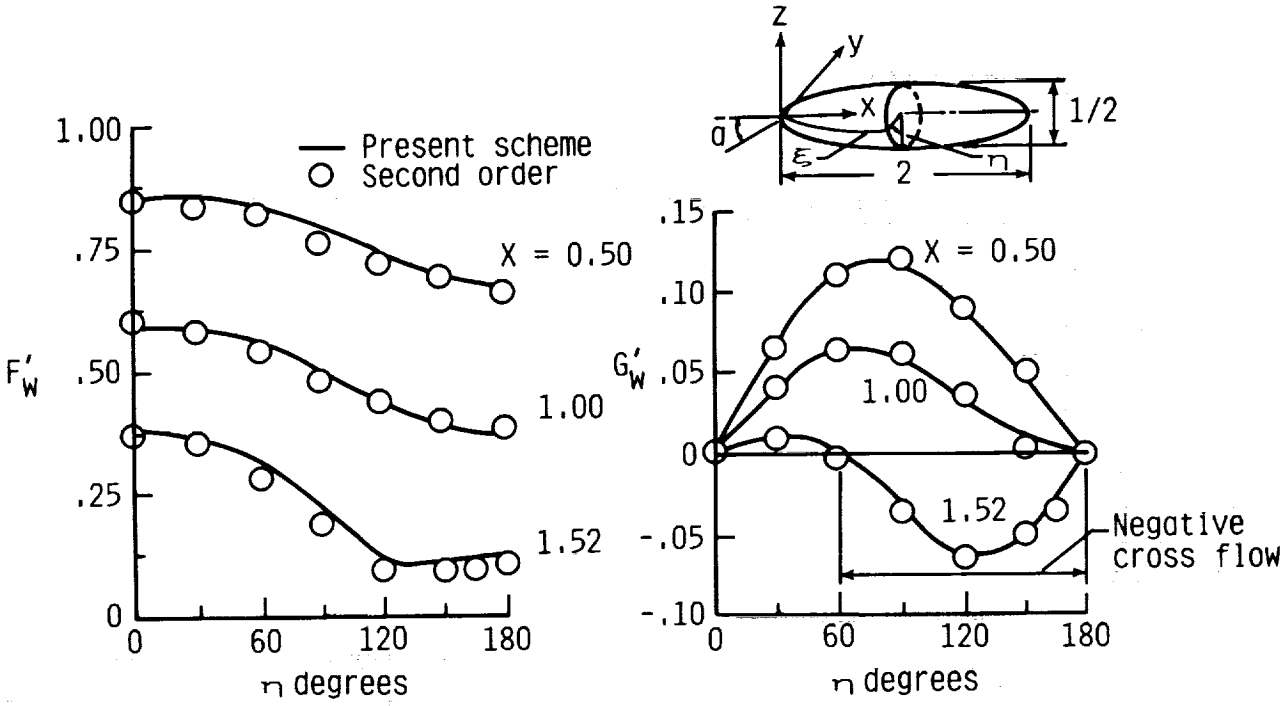

FIGURE 16

SWEPT WING FLOW

The final swept wing flow test case presented is for a wing having an NACA-0012 airfoil section. A schematic of the geometry and test conditions is presented in figure 17(a) together with calculated values of the chordwise (ξ) and spanwise (η) skin friction coefficients.

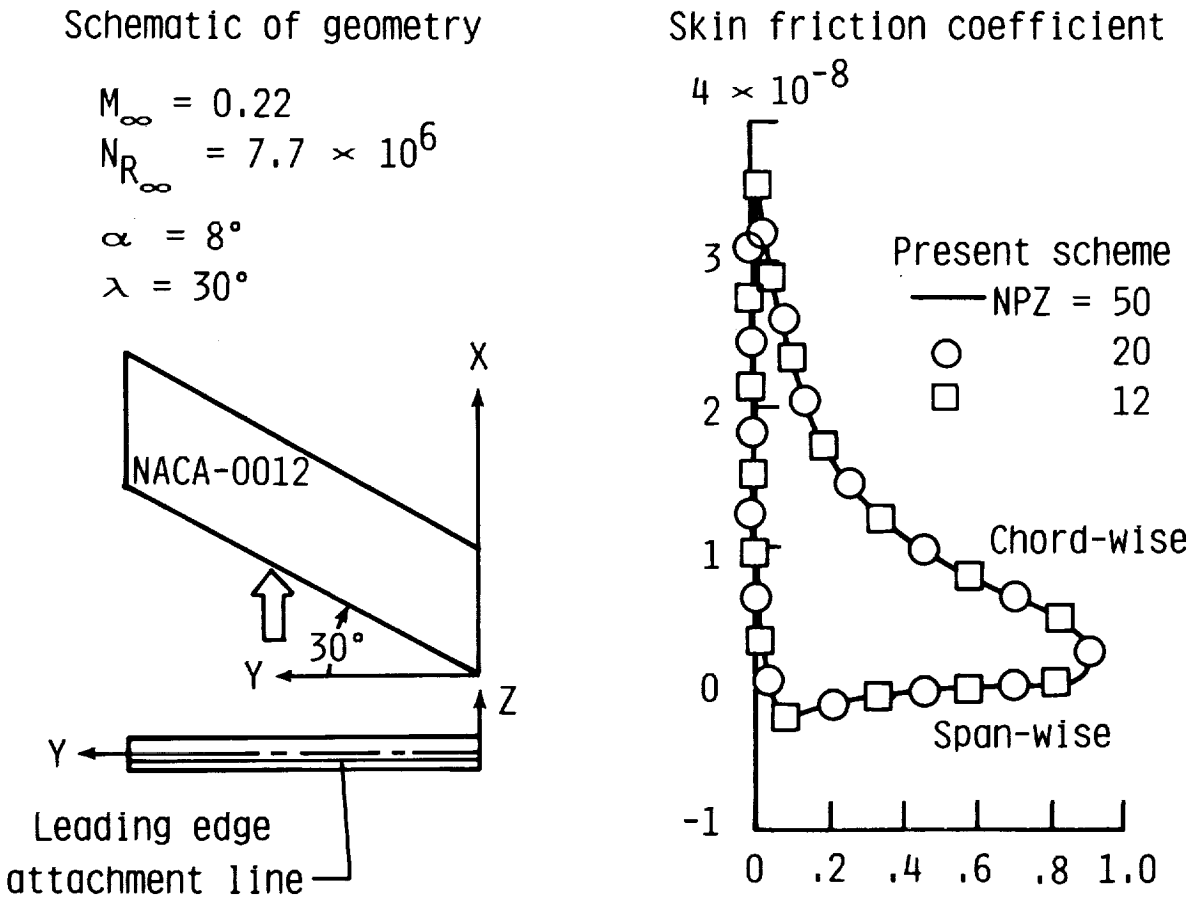

FIGURE 17(A)

SWEPT WING FLOW: VELOCITY PROFILES

Calculated total and cross flow velocity profiles are presented in figure 17(b). The numerical results were obtained for grid point distributions normal to the wall boundary of 12, 20, and 50 points. The profile calculations are presented at chord stations of 0, 50, and 90 percent. The present fourth-order method obtained accurate results with as few as 12 points normal to the wall boundary.

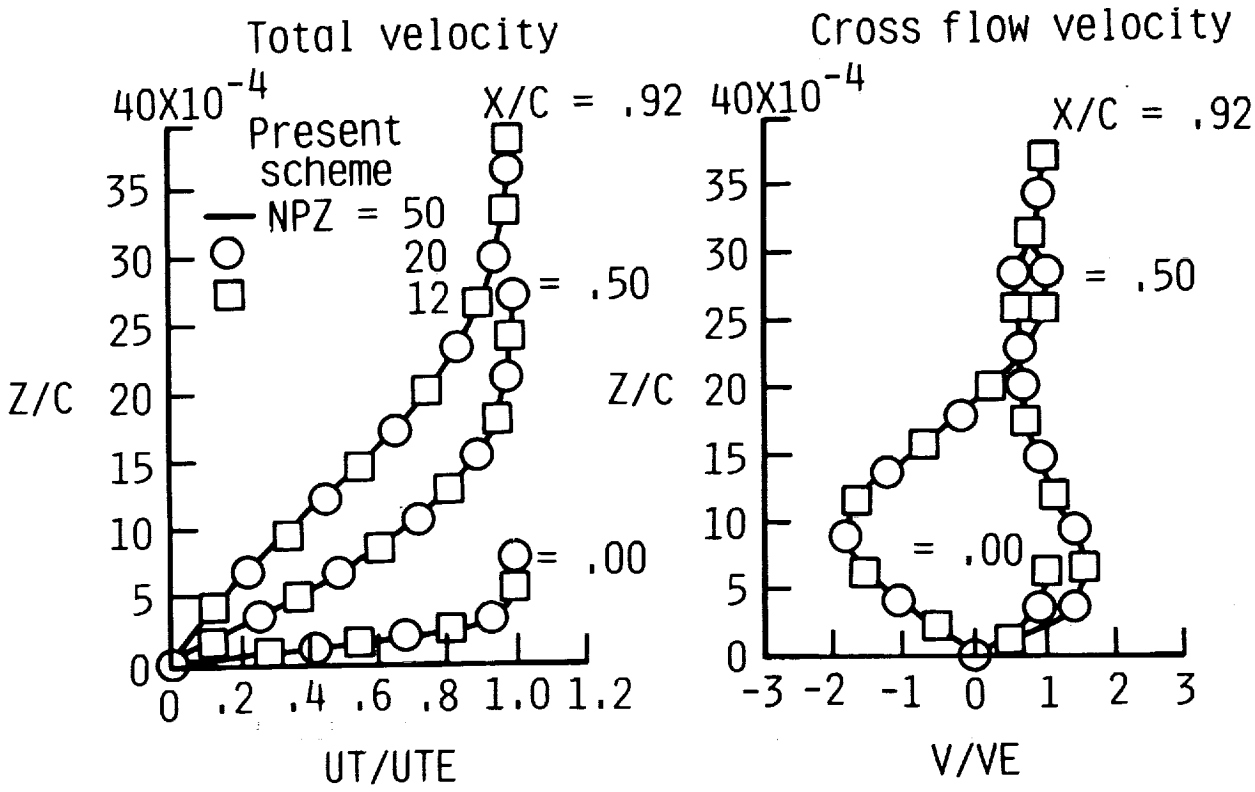

FIGURE 17(B)

CONCLUDING REMARKS

In concluding, the current software package (interface software; boundary-layer software) is operational and has been tested for several 3-D flows (see figure 18).

The interface program has been found to be a dependable approach for developing a user friendly procedure for generating the boundary-layer grid and transforming an inviscid solution from a relatively coarse grid to a sufficiently fine boundary-layer grid. The surface Euler equations used for this procedure yield smooth inviscid velocity components and gradients along the boundary-layer coordinate lines. These data are consistent with the governing equations in satisfying the boundary-layer equations in the limit as the distance normal to the wall boundary becomes very large. The interface program will eventually function as the iterative link between the selected inviscid software and the boundary-layer software for inviscid/viscous interactions studies.

The boundary-layer program has been shown to be fourth-order accurate in the direction normal to the wall boundary and second-order accurate in planes parallel to the boundary. The fourth-order accuracy allows accurate calculations with as few as one-fifth the number of grid points required for conventional second-order schemes.

- Basic programs have been developed and verified for several test cases
  - Surface Euler equation approach yields smooth and consistent inviscid edge data
  - Boundary-layer procedure has been verified as computationally efficient with fourth order accuracy

FIGURE 18

REFERENCES

1. McLean, J. D.; and Randall, J. L.: Computer Program to Calculate Three-Dimensional Boundary Layer Flows Over Wings with Wall Mass Transfer. NASA CR-3123, 1979.

2. Cebeci, T. Kaups, K.; Ramsey, J.: A General Method for Calculating Three-Dimensional Compressible Laminar and Turbulent Boundary Layers on Arbitrary Wings. NASA CR-2777, 1977.

3. Anderson, O. L.: Assessment of a 3-D Boundary Layer Analysis to Predict Heat Transfer and Flow Field in a Turbine Passage. NASA CR-174894, 1985.

4. Tassa, A.; Atta, E. H.; and Lemmerman, L. A.: A New Three-Dimensional Boundary Layer Calculation Method. AIAA-82-0224.

5. Hirschel, E. H.; and Kordulla, W.: Shear Flow in Surface-Oriented Coordinate. Notes on Numerical Fluid Mechanics, vol. 4, Friedr, Vieweg & Son, Braunschweig/Wiesbaden, 1981.

6. Cebeci, T.; and Meier, H. U.: A Note on the Specification of Freestream Velocity in the Calculation of the Boundary Layer Flow Around Bodies of Revolution at Incidence. Z. Flugwiss, Weltraumforsch 6 (1982), Heft 6, p. 416-418.

7. Vollmers, H.: Integration of Streamlines from Measured Static Pressure Fields on a Surface. AIAA 82-4236.

8. Gleyzes, C.; and Cousteix, J.: Calculation of Streamlines from Wall Pressures on a Fusiform Body. Rech. Aerosp., 1984-3, pp. 69-77.

9. Iyer, V.; and Harris, J. E.: Solution of the Surface Euler Equations for Accurate Three-Dimensional Boundary-Layer Analysis of Aerodynamic Configurations. AIAA 87-1154-CP.

10. Hess, J. L.: Calculation of Potential Flow About Arbitrary 3-D Lifting Bodies. McDonnell Douglas, MDC J5679-01, 1972.

11. Krause, E.; Hirschel, E.; and Boltman, : Numerical Stability of Three-Dimensional Boundary-Layer Solutions. Z Angew Math. and Mech., vol. 48, no. 8, pp. 205-208, 1968.

12. Radwan, S. F.; and Lekoudis, S. G.: Calculations of the Incompressible Turbulent Boundary Layer on an Ellipsoid in the Inverse Mode. AIAA Paper No. 85-1654.

13. Wornom, S. F.: Critical Study of Higher Order Numerical Methods for Solving the Boundary Layer Equations. NASA TP-1302, 1978.

14. Linger, W.; and Willoughby, R. A.: Efficient Integration Methods for Stiff Systems of Ordinary Differential Equations. SIAM J., Numer. Analysis, vol. 7, no. 1, March 1970.